OM1361 (13.61 carats; $\delta^{18}O = 22.3$, one analysis). This result contradicts the proposed origin of old mine emeralds from lost mines located in southeast Asia but validates gemological observations by Ward (*1*). The fourth old mine emerald analyzed (OM 451, 4.51 carats) has a value of 13.0 ± 0.6‰ (two analyses), which is suggestive of an origin in Afghanistan. Mines located in the Pansher valley in Afghanistan contain emeralds having $\delta^{18}O$ values ranging from 13.2 and 13.9‰ (*4*). These Afghan mines were mapped by the Soviets in 1976, but the $\delta^{18}O$ value of old mine emerald OM451 shows that these mines were already exploited at least as early as the 18th century.

The $\delta^{18}O$ values of old mine emeralds thus indicate that in the 17th and 18th centuries A.D., famous treasures found today in India, in the Topkapi Sarayi Palace and in the Markazi Bank, were constitued not only from New World stones (probably constituting the dominant fraction) but also, as previously proposed, from old Asian emeralds.

References and Notes

1. F. Ward, *Emeralds* (Gem Book Publishers, Bethesda, MD, 1993).
2. E. Gonthier, in *L'émeraude*, G. Giard, G. Giuliani, A. Cheilletz, E. Fritch, E. Gonthier, Eds. (Association Française de Gemmologie Press, Paris, 1998), pp. 27–32.
3. F. H. Forestier and D. H. Piat, in *L'émeraude*, G. Giard, G. Giuliani, A. Cheilletz, E. Fritch, E. Gonthier, Eds. (Association Française de Gemmologie Press, Paris, 1998), pp. 139–145. Indian traders use the terms old mine emeralds or Moghul emeralds to designate emeralds of exceptional color, carat weight, cut, and clarity. These stones were cut in the 17th and 18th centuries A.D., but some of them might originate from older treasures. These emeralds have an unknown origin, but they are classically advocated to come from old mines lost in the past. They are also called "Bactriane" emeralds by historians who think that they were picked up by Alexander the Great in 300 B.C. during his far eastern conquest via the Pansher Valley in Afghanistan.
4. G. Giuliani *et al.*, *Miner. Deposita* **33**, 513 (1998).
5. The *Nuestra Señora de Atocha* galleon sank on 4 September 1622 off the coast of Florida when ravaged by a hurricane [E. Lyon, *Natl.Geogr.* **149**, 786 (1976)]. In 1985, divers found the *Atocha* galleon and recovered gold, silver, and 2300 rough emeralds [E. Lyon, *Natl. Geogr.* **161**, 228 (1982)].
6. The oxygen isotopic ratios ($^{18}O/^{16}O$) of the emeralds were determined with the CRPG-CNRS Cameca 1270 ion microprobe, using a Cs^+ primary beam and electron bombardment and analyzing in monocollection mode the ^{16}O and ^{18}O secondary ions at a mass resolution of ≈4500. Cut emeralds were oriented so that flat surfaces could be sputtered. The instrumental mass fractionation was calibrated on a set of emerald standards of different compositions and different crystallographic orientations previously measured in bulk by conventional mass spectrometry (*4*). The $^{18}O/^{16}O$ ratios were determined with a precision of ≈±0.6‰ (1σ) and are reported here with $\delta^{18}O$ notation, in per mil variations relative to the international standard mean ocean water standard, whose $^{18}O/^{16}O$ ratio is 2.0052×10^{-2}. The craters produced on the emeralds were ≈10 to 20 μm in diameter and of a few angstroms depth (≈2×10^{-11} g of an emerald were sputtered for one analysis). These spots are invisible to the naked eye, so this method can be considered nearly nondestructive and can be applied to gems of high value.
7. Emerald is the mineral beryl, $Be_3Al_2Si_6O_{18}$, in which a minor amount of Cr(V) is present. Two main types of emerald deposits are recognized worldwide (*4*): Type I, which corresponds to most of the deposits, involves the intrusion of granitic pegmatites within Cr(V)-bearing mafic-ultramafics. Type II emerald forms in thrusts, faults, and shear zones in Cr(V)-bearing rocks.
8. Emeralds can be classified in three groups according to their $\delta^{18}O$ values (*4*). The first group, with 6.2‰ < $\delta^{18}O$ < 7.9‰, includes emeralds from Brazil (Quadrilatero Ferrífero and Anagé districts), Austria (Habachtal, $\delta^{18}O = 7.1 \pm 0.1$‰), Australia (Poona), and Zimbabwe (Sandawana). The second group, with 8.0‰ < $\delta^{18}O$ < 12‰, includes most of the deposits in the world; that is, those of Zambia, Tanzania, Russia, Madagascar, Egypt ($\delta^{18}O = 10.3 \pm 0.1$‰), Pakistan (Kaltharo), and Brazil (Carnaíba and Socotó). The third group, with $\delta^{18}O$ > 12‰, includes the emerald deposits of Brazil (Santa Terezinha de Goiás), Afghanistan, Pakistan (the Swat-Mingora district), and Colombia (eastern zone, $\delta^{18}O$ = 16.8 ± 0.1‰; western zone, $\delta^{18}O$ = 21.2 ± 0.5‰).
9. The mineralogical and gemological data that are normally used to determine the origin of natural emeralds are the optical features (refractive indices and birefringence), density, adsorption spectra (ultraviolet and near-infrared), internal characteristics (growth phenomena and solid and fluid inclusions), and the chemical composition. However, the diagnostic value of these data is often restricted, because there may be an overlap for emeralds originating from different localities. On the other hand, the combination of mineralogical and gemological properties can be used, in many cases, to accurately identify emeralds from specific localities. Sometimes, even certain isolated data are highly characteristic. For example, emeralds from the Brazilian deposits of Salininha and Santa Terezinha, as well those from central Nigeria, can be identified by their spectroscopic data.
10. R. Dominguez, in *Historia de las esmeraldas de Colombia* (Graficas Ducal Edition, Bogotá, Colombia, 1965), pp. 131–169.
11. J. C. H. Zwaan, J. Kanis, E. J. Petsch, *Gems Gemol.* **33**, 80 (1997).
12. D. Schwarz, in *Esmeraldas—Inclusões em gemas*, D. Schwarz and Universidade Federal Ouro Preto (UFOP), Eds. (Imprensa Universitária UFOP, Ouro Preto Publishers, 1987), pp. 304–305.
13. Y. Y. Nwe and G. Grundmann, *Lithos* **25**, 281 (1990).
14. C. Beurdeley, in *Sur les routes de la soie* (Edition Seuil, Fribourg, 1985), pp. 14–35.
15. The first Colombian emeralds in Europe were given to Hernán Cortés by the Aztec emperor Moctezuma II. These gifts were given to Charles Quint and were described by Albrecht Dürer in 1520. Some of these great samples, which were traded through Mesoamerica from the 10th century onward, are now curated at Vienna and Dresden (*16*).
16. P. Bariand and J.-P. Poirot, in *Larousse des pierres précieuses* (Librairie Larousse, Paris, 1985), pp. 133–142.
17. Primary fluid inclusions trapped in Colombian emeralds are typically brines. At room temperature, the degree of filling of the cavities is fairly constant. The inclusions typically contain a cubic crystal of halite (12 to 15 volume %), a brine (75 volume %), a vapor bubble (10 volume %), and sometimes a liquid carbonic phase (CO_2 liquid up to 3 volume %), which is easily visible in flat and large inclusions. These halite-bearing fluid inclusions are commonly used as the main criteria for diagnosis of Colombian emeralds, but they cannot be used to determine the origin more precisely to find the mine locality.
18. R. E. Kane *et al.*, *Gems Gemol.* **25**, 196 (1989).
19. Oxygen isotope analyses made with the classical fluorination technique (*4*) on the old mine emerald OM 441 gave a $\delta^{18}O$ value of 20.5 ± 0.3‰ (three analyses), which overlaps the value range defined by ion microprobe [$\delta^{18}O$ = 20.0 ± 0.8‰ (eight analyses)].

20. We thank the Mel Fisher Maritime Heritage Society in Key West, Florida, for providing a rough crystal from the *Nuestra Señora de Atocha* galleon. This is contribution CRPG-CNRS no. 1444.

6 October 1999; accepted 22 November 1999

Quantum-Critical Conductivity Scaling for a Metal-Insulator Transition

H.-L. Lee,[1] John P. Carini,[1]* David V. Baxter,[1] W. Henderson,[2] G. Grüner[2]

Temperature (*T*)- and frequency (ω)-dependent conductivity measurements are reported here in amorphous niobium-silicon alloys with compositions (*x*) near the zero-temperature metal-insulator transition. There is a one-to-one correspondence between the frequency- and temperature-dependent conductivity on both sides of the critical concentration, thus establishing the quantum-critical nature of the transition. The analysis of the conductivity leads to a universal scaling function and establishes the critical exponents. This scaling can be described by an *x*-, *T*-, and ω-dependent characteristic length, the form of which is derived by experiment.

A quantum phase transition (QPT) is a zero-temperature, generically continuous transition tuned by a parameter in the Hamiltonian at which quantum fluctuations of diverging size and duration (and vanishing energy) take the system between two distinct ground states. Examples of QPT include the integer and fractional Quantum-Hall transitions, magnetic transitions of cuprates or heavy-Fermion alloys, and metal-insulator and superconductor-insulator transitions in disordered alloys (*1*).

These transitions are intrinsically complicated because of strong interactions between electrons and the frequent presence of static disorder (*2*). However, two features specific to QPTs make them amenable to experimental and theoretical study: (i) the diverging length and time scales of the fluctuations that drive the transitions favor the use of scaling relations (*3*) in describing experimental results, and (ii) the dominance of quantum fluctuations near the

---

[1] Department of Physics, Indiana University, Bloomington, IN 47405, USA. [2] Department of Physics, University of California, Los Angeles, CA 90095–1547, USA.

*To whom correspondence should be addressed. E-mail: jcarini@indiana.edu

critical point forces a coupling between quantum dynamics and thermodynamics that may be used to interrelate the results from a variety of experimental probes, even in the absence of a complete microscopic theory (*4*, *5*). Unfortunately, explicit and convincing demonstrations of this scaling have been rare (*6*), but experiments have successfully probed the dynamics in a limited range of parameters (*7*). The scaling functions themselves have not yet been established experimentally; however, some progress has been made theoretically (*1*).

Here we report a series of experiments that tests in detail the predictions of the scaling picture of quantum-critical dynamics. We describe measurements of the temperature (T), frequency (ω), and alloy concentration (x) dependences of the electrical conductivity for Nb-Si alloys near the metal-insulator transition and then establish the existence of scaling relations directly from experimental data. Our data are consistent with the predictions of the scaling theory, and we have used simple equations to describe this scaling behavior.

The dynamical behavior near a metal-insulator critical point for which the effective electron-electron interaction is nonzero and finite (*2*) can be expressed in the form

$$\sigma(x,T,\omega) = (e^2/\hbar b^{d-2})\, g_\pm (b/\xi_x, b/l_T, b/l_\omega) \qquad (1)$$

where σ is the conductivity, d is the spatial dimension, b is an arbitrary length scale, l_T and l_ω are characteristic lengths determined by the temperature T and frequency ω, respectively, and $g_\pm$ is two dimensionless universal functions (g_+ for metallic systems and g_- for insulating ones; the functions are identical at the critical point). For example, on the metallic side of the transition, for low temperatures and frequencies ($\xi \ll l_\omega, l_T$), the conductivity in a $d = 3$ metal-insulator transition will be controlled by the alloy concentration through the quantum correlation length

$$\sigma(x,T = 0,\omega = 0) = e^2/\hbar\xi_x \propto |x - x_c|^\nu \qquad (2)$$

where ν is the correlation length exponent. Instead, if the controlling length scale is chosen to be the thermal length ($b = l_T$), the scaling form of σ for low ω can be simplified to

$$\sigma(T,x) = (e^2/\hbar l_T)\, g_\pm (l_T/\xi_x) \qquad (3)$$

where

$$l_T \propto (k_B T)^{-1/z} \qquad (4)$$

where z is the dynamical exponent and k_B is the Boltzmann constant; the frequency-dependent expressions are completely analogous, making the replacement ($k_B T \rightarrow \hbar\omega$).

To explore the scaling behavior, samples with different Nb concentrations were grown on 0.5-mm-thick sapphire substrates as described previously (*8*). The dc conductivity was measured with a standard four probes technique over a wide range of temperature (Fig. 1A). This technique helps to separate metallic samples, for which σ approaches a constant at low temperature (solid symbols), and insulating samples, for which σ falls rapidly at low temperature (open symbols). The sample represented by the open circles will establish itself as being extremely close to the transition. As seen in the inset, the conductivity varies linearly as a function of $T^{1/2}$ for the more metallic samples in the temperature range from 1.4 to 16 K.

The ac conductivity was measured at frequencies ranging from 5 to 1000 GHz. Two different techniques were used at the lower and higher frequencies, respectively. Both methods exploit the fact that when an electromagnetic wave goes through a film that is thin compared with the skin depth, the energy loss is proportional to the real part of the conductivity of the film, and the imaginary part of the conductivity gives a phase shift. At 5 and 12 GHz, measurements were made with resonant cavities (*9*). Millimeter-wave transmission measurements were done over the frequency range 80 to 1000 GHz with a quasi-optical spectrometer (*10*). The sample and substrate form a Fabry-Perot cavity

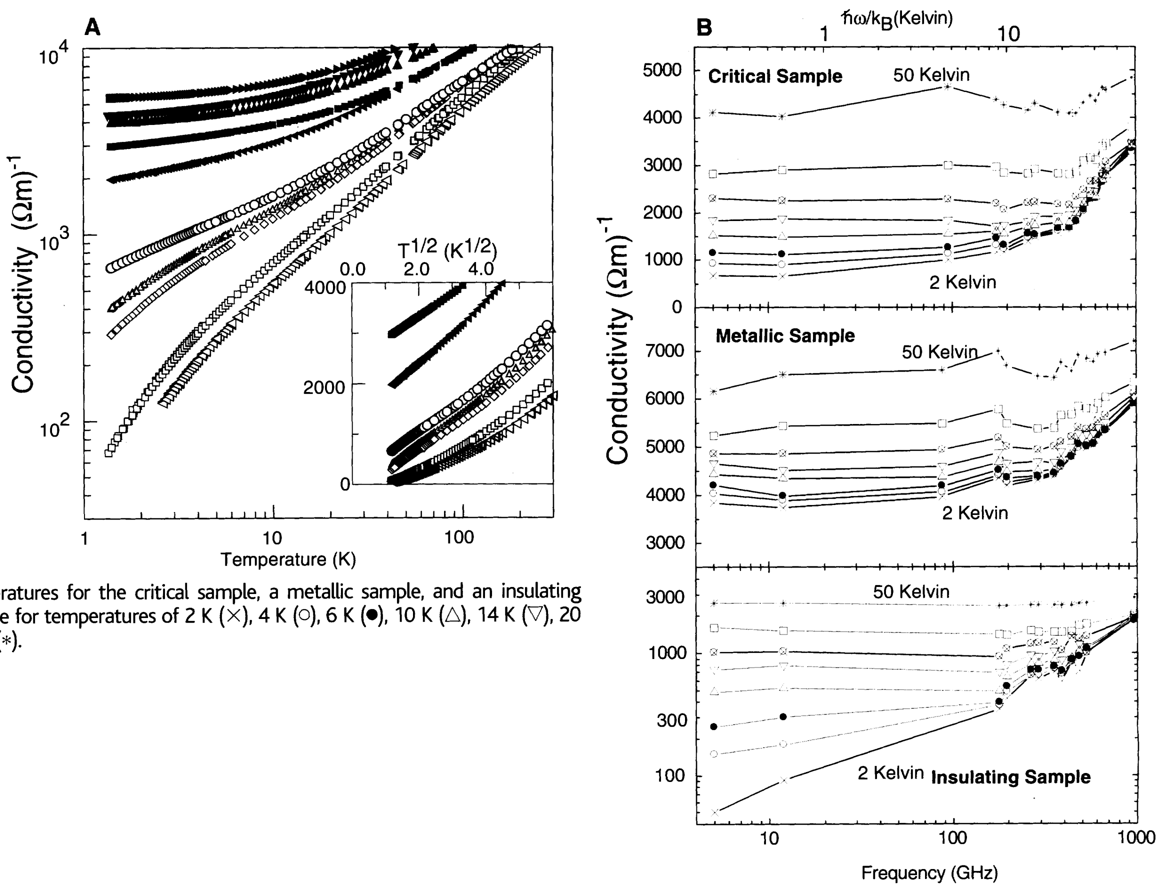

Fig. 1. (**A**) The dc conductivity for NbSi alloys with varying Nb concentration. The sample with the open circles is very close to the critical concentration, with $\sigma \propto T^{1/2}$ approaching the limit $T \rightarrow 0$ (see inset). Samples with conductivity curves above it remain metallic because the conductivity remains nonzero, whereas samples with conductivity curves below it will not conduct for $T = 0$. Solid symbols, metallic samples; open circles, critical sample; other open symbols, insulating samples. (**B**) The frequency dependence of the real part of the conductivity at several temperatures for the critical sample, a metallic sample, and an insulating sample. The data shown are for temperatures of 2 K (×), 4 K (○), 6 K (●), 10 K (△), 14 K (▽), 20 K (⊗), 30 K (□), and 50 K (*).

for the millimeter-wave radiation, and the real part of the conductivity of the film can be extracted from the magnitudes of the transmission peaks. The imaginary component of the film's conductivity can be determined at each peak by the small changes in its peak frequency.

The frequency dependence of the real part of the conductivity was measured at several temperatures for three different samples (Fig. 1B), including the critical sample and one each of the metallic and insulating samples. With the exception of a subset of the insulating sample data in which both the temperature is low ($T <$ 10 K) and the frequency is low ($\omega <$ 100 GHz), all three samples exhibit the same behavior. First, at the highest temperatures, the conductivity is frequency-independent. Second, at the highest frequencies, the conductivity tends to become temperature-independent for $T <$ 20 K.

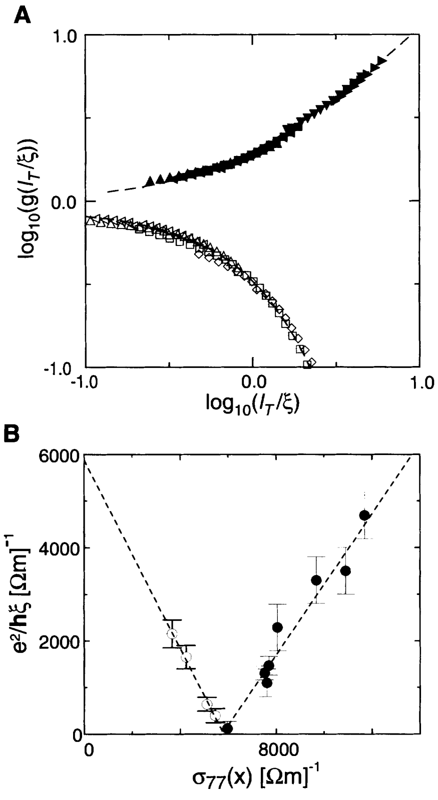

Fig. 2. **(A)** Scaling plot of the conductivity data shown in Fig. 1A with $\sigma <$ 6000(ohm · m)$^{-1}$ (includes data for samples not shown in Fig. 1A). Data on the metallic and insulating side collapse onto different scaling functions. The scaling function on the metallic side is described by $g = 1 + l_T/\xi$ (upper dashed curve) and on the insulating side is described by $g = \exp(-l_T/\xi)$ (lower dashed curve). Symbols are as in Fig. 1A. **(B)** Zero-temperature limit of the conductivity of metallic samples and the $e^2/\hbar\xi$ value for insulating samples plotted against their conductivity value at 77 K. The dotted lines are linear fits to the data, which both suggest a critical point at the concentration for which $\sigma_{77} \sim$ 5800(ohm · m)$^{-1}$. Open circles, insulating samples; solid circles, metallic samples. Error bars indicate uncertainties in the extrapolated values.

The scaling analysis presented below shows that the T-ω crossover is essentially identical for all three samples.

The objective of the scaling analysis is to describe the temperature, frequency, and composition dependences of the conductivity in one unified picture and to establish the scaling function and values for the critical exponents directly from the experimental data. We first focus on the temperature dependence and subsequently include the frequency dependence.

Using the dc conductivity data collected for each sample, $\sigma(T,x)$, we can test for the existence of a universal scaling function with Eqs. 2, 3, and 4

$$g_{\pm}\left[\frac{\sigma(0,x)}{\sigma(T,x_c)}\right] = \frac{\sigma(T,x)}{\sigma(T,x_c)} \qquad (5)$$

Figure 2A was constructed using Eq. 5, with the data from the sample with the open circles in Fig. 1A representing the critical behavior, $\sigma(T,x_c)$. If we consider only data with $\sigma \leq$ 5000(ohm · m)$^{-1}$, all the data on the metallic side of this sample collapse into one curve. Substituting as the critical set the data from samples just above or below this one does not produce such a collapse. Therefore we conclude that we have identified a sample that is very close to the critical concentration. From its conductivity we find $l_T \propto T^{-1/2}$ and $z = 2$.

A simple function describes the shape of the scaling function on the metallic side

$$g_+(l_T/\xi) = 1 + l_T/\xi \qquad (6)$$

that is consistent with the expected limiting behaviors of Eq. 3 (illustrated by the upper dashed line in Fig. 2A). On the insulating side, the data can be collapsed to a single curve by dividing by the critical data set and attempting to combine into a single function

$$g_-(l_T/\xi) = \exp(-l_T/\xi) \approx (1 + l_T/\xi)^{-1} \qquad (7)$$

and adjusting the value of ξ for each sample. The approximate form emphasizes the duality in $g_{\pm}(y)$ for $y \ll 1$. This exponential function used to align the data sets (shown by the lower part of the dashed line in Fig. 2A) describes the collapsed data. The exponential function and Eq. 4 imply that the conductivity on the insulating side has a temperature dependence $\sigma(T,x) \propto T^{1/2}\exp[-(T_0/T)^{1/2}]$, which is similar to the Efros-Shklovskii variable range hopping conductivity formula that often describes the temperature dependence of the conductivity of disordered insulators deep in the insulating phase of disordered systems (*11*).

Both the values of $\sigma(x,T = 0)$ (for metallic samples) and $e^2/\hbar\xi(x)$ (for insulating samples) vary linearly with the sample conductivity at 77 K, σ_{77} (Fig. 2B). Assuming that the high-temperature conductivity varies linearly with Nb concentration, this indicates that ξ depends on concentration, according to Eq. 2 with $\nu \simeq 1$ on both sides of the transition. This value of ν is in agreement with earlier results of the transport and tunneling measurements on Nb-Si alloys (*12*) conducted on the metallic side but is inconsistent with what is expected for a disorder-driven transition with no interactions (the Anderson transition), where $\nu \approx 1.35$ according to scaling analysis of numerical simulations of the critical behavior (*13*). This is gratifying because our observation of the scaling itself emphasizes the importance of electron-electron interactions at the transition (*1*).

Scaling theory also requires a close relation between the effects on the conductivity of fluctuations sampled directly (by $\hbar\omega$) and those driven by thermal excitations (k_BT). To test this idea with our data, we directly compared the T dependence for the three samples from Fig. 1B to their ω dependence at 2 K (at which $\hbar\omega > k_BT$) (Fig. 3A). The frequency (in hertz) has been scaled by $h/1.54k_B$ and the critical sample shows both $\sigma(T = 0,\omega) \propto \omega^{1/2}$ and $\sigma(T,\omega = 0) \propto T^{1/2}$, which are in agreement with the predictions of quantum-critical scaling (*8*).

Continuing with scaling, we defined a new length scale $l_{T,\omega} = l_T/\Sigma(\hbar\omega/k_BT)$ and a scaling form for the real part of the conductivity

$$\sigma_1(x,T,\omega) = (e^2/\hbar l_{T,\omega})g(l_{T,\omega}/\xi) \qquad (8)$$

The function Σ approaches 1 for $\hbar\omega \ll k_BT$ and approaches $(\hbar\omega/k_BT)^{1/2}$ for $\hbar\omega \gg k_BT$, with a rapid crossover for $\hbar\omega \approx k_BT$. With this form of the scaling hypothesis, we are able to collapse the ac data from various temperatures onto the same curve (Σ) for all three samples from Fig. 1B (Fig. 3B). For the critical sample, the dc data may be used to determine $l_T = e^2/\hbar CT^{1/2}$ where $C = 475$ (ohm · mK$^{1/2}$)$^{-1}$ is a constant and hence we expect $\Sigma = \sigma/CT^{1/2}$ (Fig. 3B, top). For the sample on the metallic side of the transition, we may use Eq. 6 to find $\Sigma = (\sigma - \sigma_0)/CT^{1/2}$, where $\sigma_0 = 2900$ (ohm · m)$^{-1}$ (from the low T limit of the 5-GHz data in Fig. 1B). Finally, for the insulating sample, we use the approximate form in Eq. 7 for g_- and solve for Σ in Eq. 8, giving

$$\Sigma(\hbar\omega/k_BT) = (\sigma l_T/2G_0)[1 + (1 + 4G_0/\sigma\xi)^{1/2}] \qquad (9)$$

where $G_0 = 0.03e^2/h$ is a constant.

For low temperatures, the data for all three samples collapse onto a single curve, which is approximated by the real part of a complex expression (solid line in Fig. 3B)

$$\Sigma(\hbar\omega/k_BT) = \mathrm{Re}\{[1 + b(-i\hbar\omega/k_BT)^a]^{1/2a}\} \qquad (10)$$

where $a \approx 1.1$ and $b \approx 1.3$. This indicates that Eq. 8 correctly describes the behavior of the conductivity, provided that the temperature is less than 25 K and the frequency is less than 500 GHz.

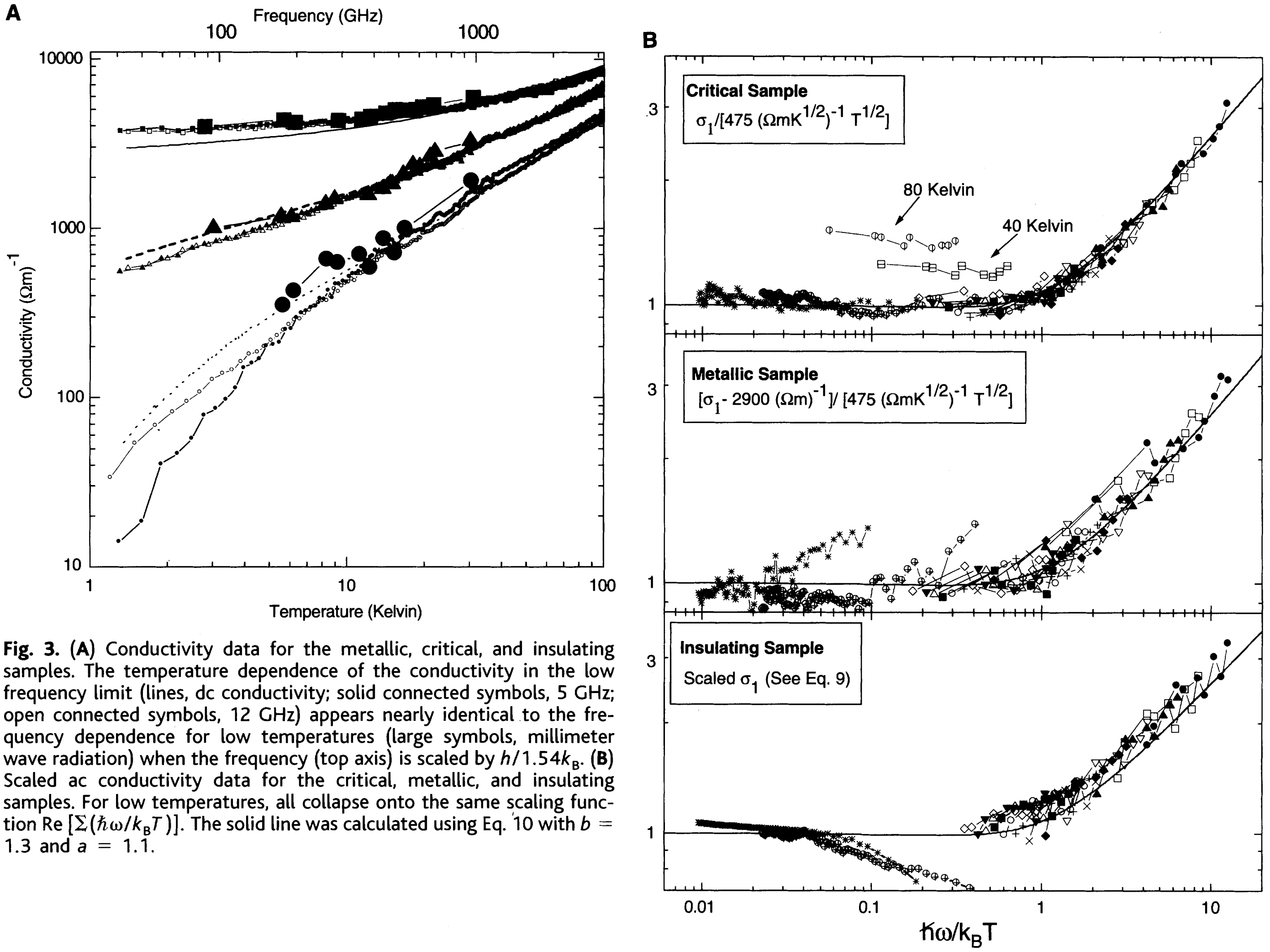

Fig. 3. (**A**) Conductivity data for the metallic, critical, and insulating samples. The temperature dependence of the conductivity in the low frequency limit (lines, dc conductivity; solid connected symbols, 5 GHz; open connected symbols, 12 GHz) appears nearly identical to the frequency dependence for low temperatures (large symbols, millimeter wave radiation) when the frequency (top axis) is scaled by $h/1.54k_B$. (**B**) Scaled ac conductivity data for the critical, metallic, and insulating samples. For low temperatures, all collapse onto the same scaling function Re $[\Sigma(\hbar\omega/k_BT)]$. The solid line was calculated using Eq. 10 with $b = 1.3$ and $a = 1.1$.

The temperature-frequency correspondence (Fig. 3A) and the scaling results imply that on both sides of the transition, the interplay between frequency and temperature can be described by the parameter $l_{T,\omega}$, which is controlled by the ratio $\hbar\omega/k_BT$ as predicted by quantum-critical scaling. Using Eqs. 8 and 10 with $b = 1.3$, we have $l_{T,\omega} = l_T$ for $\omega \ll k_BT/\hbar$ and $l_T = (\hbar\omega/1.54k_BT)^{1/2}$ for $\omega \gg k_BT/\hbar$. Thus, for $\hbar\omega = 1.54k_BT$, $l_{0,\omega} = l_{T,0}$, which is consistent with the scaling between k_BT and $\hbar\omega$ used to demonstrate the temperature-frequency correspondence (Fig. 3A).

Our experiments imply the existence of simple scaling functions. From the length scale (L) dependence of the scaling function $g_+(L, \xi) = 1 + L/\xi$, we can independently determine the correlation length exponent from its derivatives $\nu^{-1} = d\beta/d\ln g|_{g_c}$, where $\beta = d\ln g/d\ln L$ and $\beta(g_c) = 0$ defines the critical value. We find $\beta = 1 - 1/g$, $g_c = 1$ and discover that ν must equal 1. We draw two conclusions: (i) the particular form of the scaling function that describes our data is consistent with the observed value for the correlation length exponent, and (ii) it is likely that the simplicity of the scaling functions we have found will not be a general feature of all QPTs.

We have determined the scaling function and the critical exponents that govern the conductivity dynamics on both sides of a QPT in a disordered, interacting electron system. The frequency dependence of the complex conductivity establishes the quantum-critical nature of the transition at which electron-electron interactions remain nonzero and finite. We argue that the simple scaling functions are consistent with the specific values of the correlation length exponent as determined from the data. It remains to be seen whether the same formalism can also account for other dynamical experiments such as electric-field–dependent conductivity studies or wave-vector–dependent conductivity studies, which could reveal further relationships between the temporal and spatial fluctuations.

References and Notes

1. S. Sachdev, *Quantum Phase Transitions* (Cambridge Univ. Press, New York 1999).
2. D. Belitz and T. R. Kirkpatrick, *Rev. Mod. Phys.* **66**, 261 (1994).
3. F. J. Wegner, *Z. Phys B* **25**, 327 (1976).
4. E. Abrahams and G. Kotliar, *Science* **274**, 1853 (1996).
5. S. L. Sondhi, S. M. Girvin, J. P. Carini, D. Shahar, *Rev. Mod. Phys.* **69**, 315 (1997).
6. L. W. Engel *et al.*, *Phys. Rev. Lett.* **71**, 2638 (1993); however, see also N. Q. Balaban *et al.*, *Phys. Rev. Lett.* **81**, 4967 (1998).
7. For example: A. Husmann *et al.*, *Science* **274**, 1874 (1996); G. Aeppli, T. E. Mason, S. M. Hayden, H. A. Mook, J. Kulda, *Science* **278**, 1432 (1997); T. Valla *et al.*, *Science* **285**, 2110 (1999).
8. H. L. Lee, J. P. Carini, D. V. Baxter, G. Grüner, *Phys. Rev. Lett.* **80**, 4261 (1998).
9. G. Grüner, in vol. 74 of *Millimeter and Submillimeter Wave Spectroscopy of Solids, Topics in Applied Physics*, G. Grüner, Ed. (Springer-Verlag, New York, 1998).
10. A. Schwartz *et al.*, *Rev. Sci. Instrum.* **66**, 2943 (1995).
11. A. L. Efros and B. I. Shklovskii, in *Electron-Electron Interactions in Disordered Systems*, A. L. Efros and M. Pollak, Eds. (Elsevier, New York, 1985).
12. G. Hertel, D. J. Bishop, E. G. Spencer, J. M. Rowell, R. C. Dynes, *Phys. Rev. Lett.* **50**, 743 (1983); D. J. Bishop, E. G. Spencer, R. C. Dynes, *Solid-State Electron* **38**, 73 (1985).
13. E. Hofstetter and M. Schreiber, *Europhys. Lett.* **21**, 20 (1993).
14. We thank E. Abrahams, S. Girvin, A. Kapitulnik, and S. Sachdev for comments on this work. Research at Indiana was supported by NSF grants DMR-9314018 and DMR-9423088; research at UCLA was supported by NSF grant DMR-9801816.

10 August 1999; accepted 24 November 1999